Characterisation of turbulent flow and the wake of a tidal stream turbine in proximity to ridges of differing length

Sulaiman Hurubi, Tim Stallard, Peter Stansby, Hannah Mullings, and Pablo Ouro

Abstract—**Fast tidal currents are generally found in shallow water depths where tidal turbines can be deployed to operate. In complex environments in which there is an irregular bathymetry, seabed shape changes can induce pressure gradients that accelerate or decelerate the flow depending on the slope and relative depth, affecting turbine wake recovery. In this study, a laboratory scale turbine, represented numerically using an Actuator Line Method (ALM), is computed using Large-Eddy Simulation (LES) over a flat-bed and in presence of three ridges with differing streamwise lengths. Turbines are positioned at several locations, namely at ridge-centre ($0D$) and at $2D$ upstream and downstream from the foot of the ridge to establish the influence of location on wake recovery rate. Turbine operating point is selected to yield a constant tip-speed ratio based on the disc-averaged velocity at each location obtained from a precursor simulation run without turbines. Results show that, relative to the same turbine in a flat channel, there is a noticeable enhancement of the rate of wake recovery when a turbine is sited upstream of the ridge whereas fatigue loads are higher when sited downstream of the ridge. Implications for array design regarding performance losses due to turbine- and bathymetry-induced wakes are drawn.**

Index Terms—**Tidal stream turbine, Bathymetry, Large-eddy simulations, Wake recovery.**

Part of a special issue for EWTEC 2023. Original version published in EWTEC 2023 proceedings at https://doi.org/10.36688/ewtec-2023-464.

Manuscript submitted 20 December 2024; Accepted 8 January 2025. Published 31 May 2025.

This article has been subject to single blind peer review by a minimum of two reviewers.

The study was partly supported by funding from the Engineering and Physical Sciences Research Council (EPSR) Supergen Offshore Renewable Energy Hub (EP/Y016297/1)

Sulaiman Hurubi. School of Engineering, University of Manchester, Manchester, M13 9PL, UK (e-mail: sulaiman.hurubi@postgrad.manchester.ac.uk), and Department of Civil and Architectural Engineering, Jazan University, Jazan 45142, Saudi Arabia.

Tim Stallard. School of Engineering, University of Manchester, Manchester, M13 9PL, UK (e-mail: tim.stallard@manchester.ac.uk).

Peter Stansby. School of Engineering, University of Manchester, Manchester, M13 9PL, UK (e-mail: peter.stansby@manchester.ac.uk).

Hannah Mullings. School of Engineering, University of Manchester, Manchester, M13 9PL, UK (e-mail: hannah.mullings@manchester.ac.uk).

Pablo Ouro. School of Engineering, University of Manchester, Manchester, M13 9PL, UK (e-mail: pablo.ouro@manchester.ac.uk).

Digital Object Identifier: https://doi.org/10.36688/imej.8.91-99

I. INTRODUCTION

TIDAL stream power generation has been shown to offer a reliable and consistent source of energy due to its predictable and cyclic nature. However, fast tidal currents are mostly located in shallow water depths locations. In these conditions, the vertical extent of the water column is constrained by the water surface and seabed bathymetry. The interaction between tidal currents and the seabed can result in complex flow patterns, i.e. the generation of coherent flow structures [1], that can impact the performance and wake recovery rate of tidal turbines. These effects are important to account for in future multi-row tidal arrays as the spacing between rows could vary between deployment locations within the same site based on the local bathymetry.

Tidal energy sites may exhibit complex bathymetric features with considerable spatial variation in current and turbulence properties [1]. In Ramsey Sound (Pembrokeshire, Wales, UK), Harrold and Ouro [2] show that there is a variation in flow speed during ebb and flood tidal phases at a turbine location, which is partly attributed to the irregular bathymetry found there. The bathymetry map shows that there are ridge-like bed features just over 5 diameters from the turbine location. This sudden change in site bathymetry surrounding the turbine location in Ramsey Sound results in different velocity and turbulence intensity values during a full tidal cycle [3]. Moreover, high energy tidal sites in the Alderney Race (Raz Blanchard in French) are studied by Bourgoin et al. [4], and it was found that large flow structures and high turbulence are generated over rocky plateaus and dune crests.

In a full tidal cycle, tidal turbines located upstream of an obstacle, e.g. ridge or pinnacle, during one tidal phase will develop a wake affected by the bathymetry-induced favorable pressure gradient (FPG) that may accelerate wake recovery, as observed in wind turbines that operate upstream of a hill [5]–[8]. Whereas in the reversed flow direction, the ridge is located upstream of the turbine generating a wake that can affect the turbine's unsteady loading and also the recovery of the turbine's wake. Such effects depend on the relative distance between the device and bed form [6]. These changes in flow conditions can cause the turbines to be exposed to high levels of fatigue loads [9]. Thus, turbine deployment locations need to account for the effect of bathymetry features during the two phases of the tidal cycle, i.e. balancing a faster wake recovery when the obstacle is downstream with loading increase when in the reversed flow.

Until now, the majority of research conducted on tidal stream turbines has focused on the analysis of uniform flat bed conditions, with little attention given to turbulence induced by variations in bathymetry [1], [10]–[13]. However, it is worth noting that bathymetry-induced turbulence can actually be beneficial in terms of wake recovery rate, as it enhances turbulent transport of momentum [14]–[16]. Considering irregular terrains, a flow speed-up occurs on hill/ridge tops, which has been reported to be advantageous for wind turbines sited in those locations [17]. However, turbine wakes in these locations are found to show a slower wake recovery compared to flat terrain, which is attributed to the adverse pressure gradient (APG) present on the downstream side of the ridge slope [5]. Therefore, it is important to characterise the effect that steep and elongated ridges can have on tidal turbine wakes in such locations where the APG side of the ridge is far from the FPG side.

In this work, a high-fidelity Large-Eddy Simulation (LES) code is employed to evaluate the wake recovery of a tidal stream turbine operating in proximity to idealised ridges with differing lengths. The aim of this study is to identify how ridge length and turbine location drive the wake recovery behind the turbine when comparing with a flat-bed case.

II. NUMERICAL METHODS

To accurately quantify the contribution of ridge-induced pressure and turbulent stresses to the recovery of a tidal turbine's wake, high-fidelity Large-Eddy Simulations (LES) are performed using the Digital Offshore Farm Simulator (DOFAS) [18], an in-house code which has been validated for open channel flows and the flows downstream of tidal stream turbines [10], [19].

DOFAS employs staggered-storage of velocities on Cartesian grids and stores pressure in the cell centre, with full parallelisation using a Message Passing interface (MPI) to ensure computational efficiency. The solver resolves the spatially filtered Navier-Stokes equations for unsteady and incompressible viscous flows. The convection and diffusion terms in the Navier-Stokes equations are discretised using a second-order central difference scheme, and a low storage two-step Runge-Kutta method is used to advance simulations in time. Predicted velocities are corrected using a Poisson pressure equation with a multi-grid technique following a fully explicit fractional step method. For this study the wall-adapting local-eddy viscosity (WALE) sub-grid scale model [20] is used to approximate the unresolved anisotropic flow scales.

The Immersed Boundary Method (IBM) is used in DOFAS to efficiently represent static geometries such as ridges, and turbine hub and tower. This discrete approach is based on the direct forcing method [21]. Velocities and forces are interpolated using the ϕ_3 delta function of Roma et al. [22] with three neighbours in each direction to reduce computational overhead.

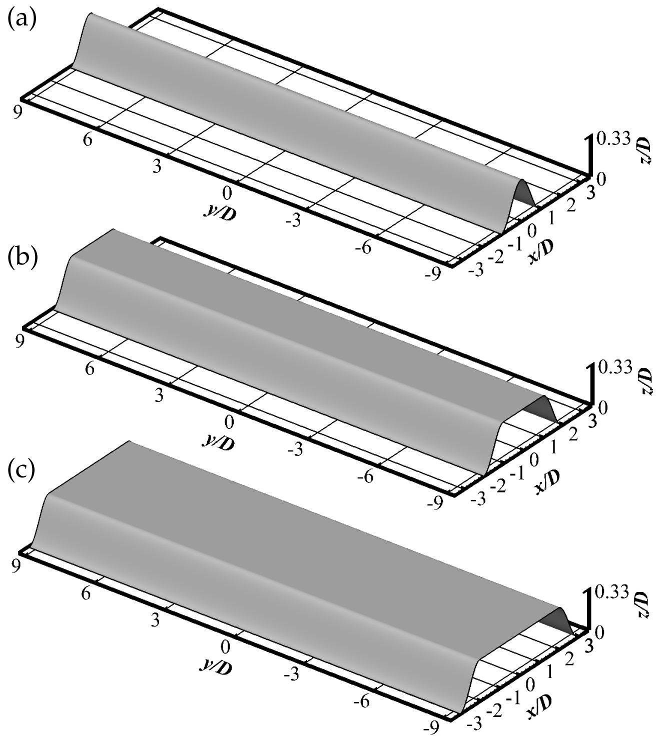

Fig. 1. Representation of the idealised ridge-type bathymetries used in cases with length of (a) $2DR$, (b) $4DR$ and (c) $6DR$.

The Actuator Line Method (ALM) adopted in DOFAS divides turbine blades into lines of moving Lagrangian markers along the blade length based on grid resolution with the use of a tip-loss correction of Prandtl-type [23]. The interpolation process is performed using a non-isotropic Gaussian projection [24].

III. DESCRIPTION OF TEST CASES

The laboratory-scale tidal stream turbine from Stallard et al. [25] is considered in this work, as this was previously validated with DOFAS using the same experimental flow conditions [18], [19]. Herein, a flat-bed simulation is run initially using a depth-averaged velocity (U_0) of 0.47 m·s^{-1} that is distributed vertically following the smooth logarithmic distribution in the experiment with a channel depth of 0.45 m. The turbine has a diameter (D) of 0.27 m and the hub height is centred at the channel mid depth connected to a bottom-fixed vertical tower. The turbine in this case operates at a rotational speed of 15.7 rad·s^{-1}, corresponding to an optimal Tip Speed Ratio (TSR) of 4.43. At this ratio, the resultant thrust and power coefficient are 0.84 and 0.3, respectively [25].

To compare the wake characteristics between flat and complex seabed bathymetry, three ridges with symmetric shapes are chosen as fundamental analysis on the impact of terrain complexity on tidal stream turbines. Fig. 1 shows symmetric ridges of differnt lengths used herein starting with $2D$ for the Gaussian-shape ridge shown in Fig. 1a. The ridge slope is characterised by the following equation:

$$Z(x) = \frac{1}{2}h\left[1+\cos\left(\frac{\pi x}{l}\right)\right] \quad (1)$$

TABLE I
DISC-AVERAGED OF NORMALISED MEAN VELOCITY (U_D), TURBULENCE INTENSITY (u'_D) OBTAINED IN THE FLAT-BED CASE AND THE THREE RIDGES AT THE SIMULATED TURBINE POSITIONS. LAST COLUMN SHOWS THE ADOPTED ROTATIONAL SPEED (Ω) BASED ON THE U_D VALUE AT EACH POSITION SUCH THAT THE TURBINE DEVELOPS THE SAME TIP SPEED RATIO AT EACH POSITION.

	$Flat$		
Position	U_D/U_0 -	u'_D/U_0 %	Ω rad s^{-1}
TF	1.01	7.56	15.7
	Ridge geometry: $2DR$		
T2U	1.02	7.44	15.7
T2C	1.19	7.45	18.9
T2D	1.16	12.76	17.8
	Ridge geometry: $4DR$		
T4U	1.02	7.60	15.7
T4C	1.23	7.55	19.1
T4D	1.11	12.42	17.4
	Ridge geometry: $6DR$		
T6U	1.01	7.92	15.7
T6C	1.24	7.81	19.1
T6D	1.07	11.54	17.3

Here, $h = H - 1.67D$ represents the height of the ridge, and l is the horizontal length of the slope. The resultant mean slope angle is 27.6°, whereas the local maximum angle is 18.4°. By keeping constant ridge slope at the upstream and downstream sides, ridge length is elongated by applying a flat top reaching a total length of $4D$ and $6D$ for the other tested ridges as illustrated in Fig. 1. The ridge centre is located at $15D$ from the inlet in all cases. The same setup of the flat-bed case is applied for ridge cases, however, the channel depth is adjusted for the cases with a ridge to ensure similar depth-to-diameter (H/D) ratio of $1.67D$ at the highest point of the ridge to the flat-bed case.

For each ridge, three turbine positions are selected. The first is located at a distance of $2D$ upstream of the ridge foot (labelled as "Turbine Upstream", TU), the second is at the ridge centre on the crest (labelled as "Turbine Centre", TC), and a third position that is identical to the first one downstream of the ridge (labelled as "Turbine Downstream", TD). These positions are selected so that they account for the ebb and flood phases of a tidal cycle in which the tidal stream turbine would face the flow from two directions relative to the ridge position, e.g. in one tidal flow direction the ridge is downstream of the turbine and vice versa. The hub height is constant at $0.83D$ from the local bottom bathymetry.

In order to maintain the same tip speed ratio to that in the flat-bed case, the rotational speed is adjusted based on the disc-averaged velocity (U_D) calculated at the turbine position from the precursor simulations performed without turbines. The disc-averaged velocity U_D is computed over the rotor swept area as:

$$U_D = \frac{1}{A_D} \sum U(x, y, z) dy dz, \quad (2)$$

where A_D is disc area and $U(x, y, z)$ is the time-averaged streamwise velocity at the cell whose dimensions are dy and dz in the lateral and vertical directions, respectively, and located within the disc. Table I shows the normalised disc-averaged velocity, turbulence intensity and the adopted rotational speed so that turbines operate at their optimal tip speed ratio for all locations in the flat-bed and ridge cases.

The simulation domain has dimensions of $49D$ in the streamwise direction and $18.5D$ in the spanwise direction. However, in the vertical direction, the flat-bed case has a depth of $1.67D$, while the ridge cases have a depth of $2D$. Simulations are run for 225 s with a fixed time step of 0.001 s and a uniform grid resolution of 0.005 m that leads to a total of 237.6 and 285.12 million grid point in the flat and ridge cases, respectively. The time step and grid resolution used in this study have been previously demonstrated to yield accurate results for flow statistics and the hydrodynamic coefficients of the turbine used here [19].

The inflow velocity distribution, with a depth-averaged velocity of $U_0 = 0.47$ m s^{-1}, is computed using a logarithmic distribution, as obtained in experiments [25], with a friction velocity ($u_\star$) equal to 0.0187 m s^{-1}. A Synthetic Eddy Method (SEM) is used to numerically superimpose artificial turbulence at the inlet with an intensity $I_x = 15\%$, which decreased further downstream to a nearly constant level of 7% along the channel, and turbulence length scales of $0.56H$, $0.33H$ and $0.25H$ in the streamwise, spanwise and wall-normal directions, respectively. A convective outflow boundary condition is set at the outlet, whereas the top surface is treated with a shear-free slip condition. The spanwise boundaries are set to periodic boundary conditions in order to decrease the lateral blockage compared to the use of walls, and a smooth-bed wall function is used at the bottom surface where the grid resolution in wall units is approx. 55 [19].

IV. RESULTS

A. Flow over ridges

The mean velocity distribution in the ridge cases with no turbine is shown in Fig. 2. In all ridge cases, the flow accelerates over the upstream slope. This is due to the favourable pressure gradient induced by the ridge [5]. Over the ridge top, it is observed that the accelerated flow persists above the elongated flat surface when ridge length is increased. On the downstream side of the ridge, a recirculation region is developed with negative values of U/U_0. The flow on the downstream side of the ridge exhibits the fundamental characteristics of a separated flow, which are similar to those observed in studies of backward facing steps [26].

Fig. 3 presents the vertical profiles of the mean velocity, turbulence intensity and vertical Reynolds shear stress at different downstream positions from the ridge centre, with vertical coordinates normalised to the origin ($z/D = 0$) at hub height. As seen in Fig. 3, turbines to be deployed upstream of the ridges (TU) are subjected to a similar streamwise velocity distribution

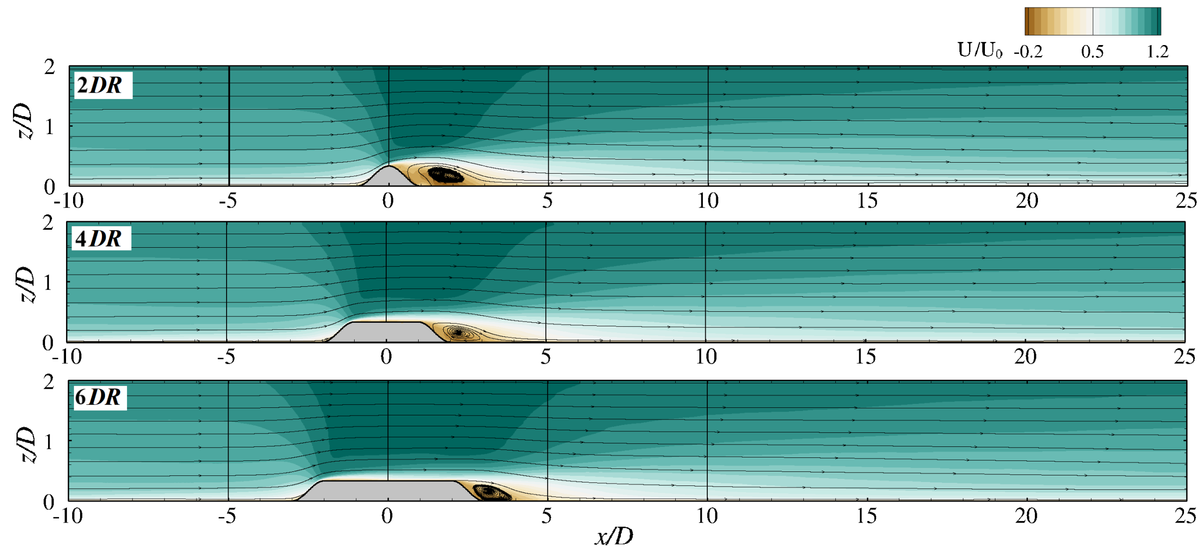

Fig. 2. Normalised mean streamwise velocity contours over $xz-$plane for the ridge cases going through the channel centre. The center of the ridge is used as a local coordinate reference in the $x-$axis.

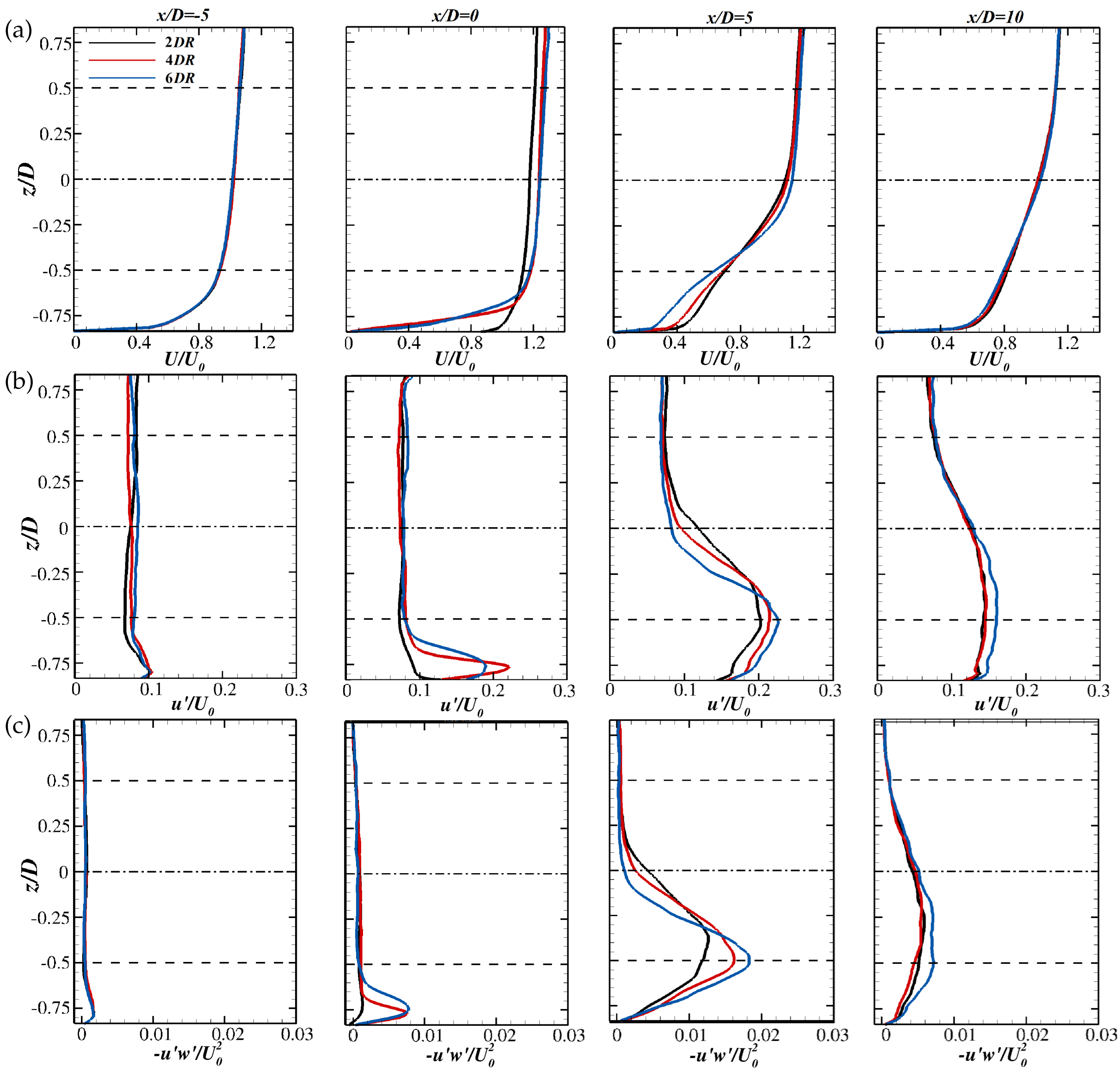

Fig. 3. Vertical profiles of (a) mean streamwise velocity, (b) turbulence intensity and (c) Reynolds shear stress at different locations as indicated with black lines in Fig. 1. Black dashed line shows the turbine area and turbine centre is used as a local coordinate reference in the $z-$axis.

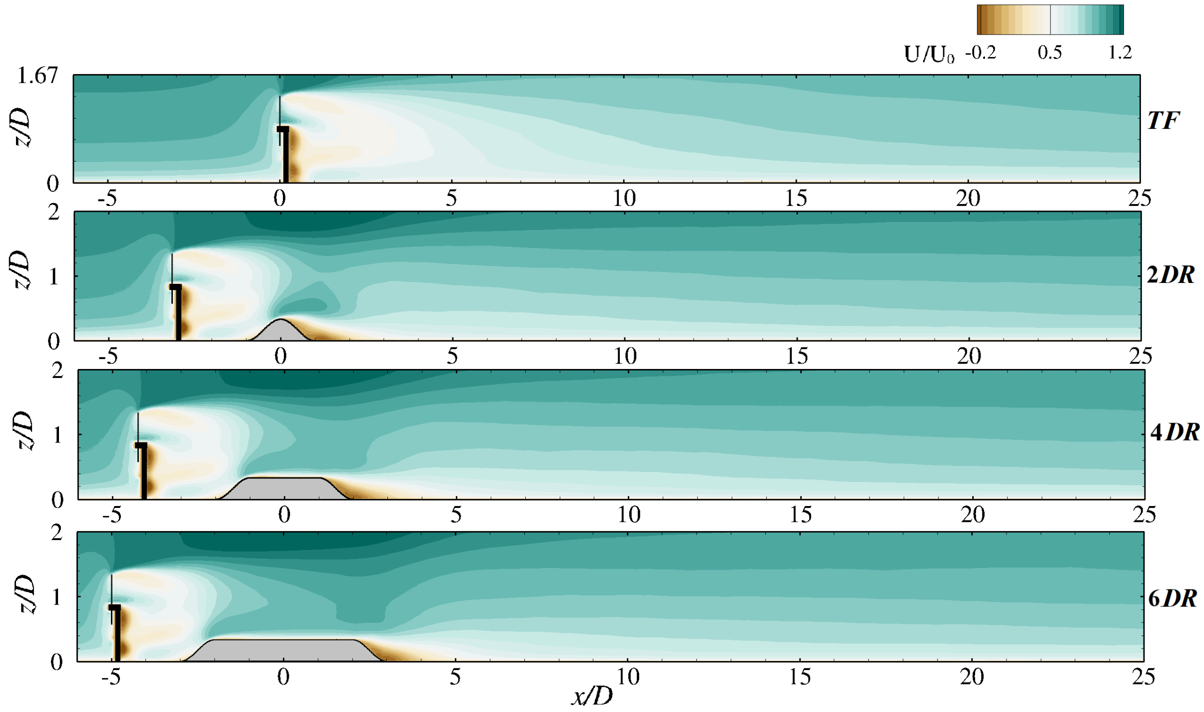

Fig. 4. Normalised mean streamwise velocity contours over $xz-$plane for the flat-bed case and upstream turbines (TU) in the ridge cases.

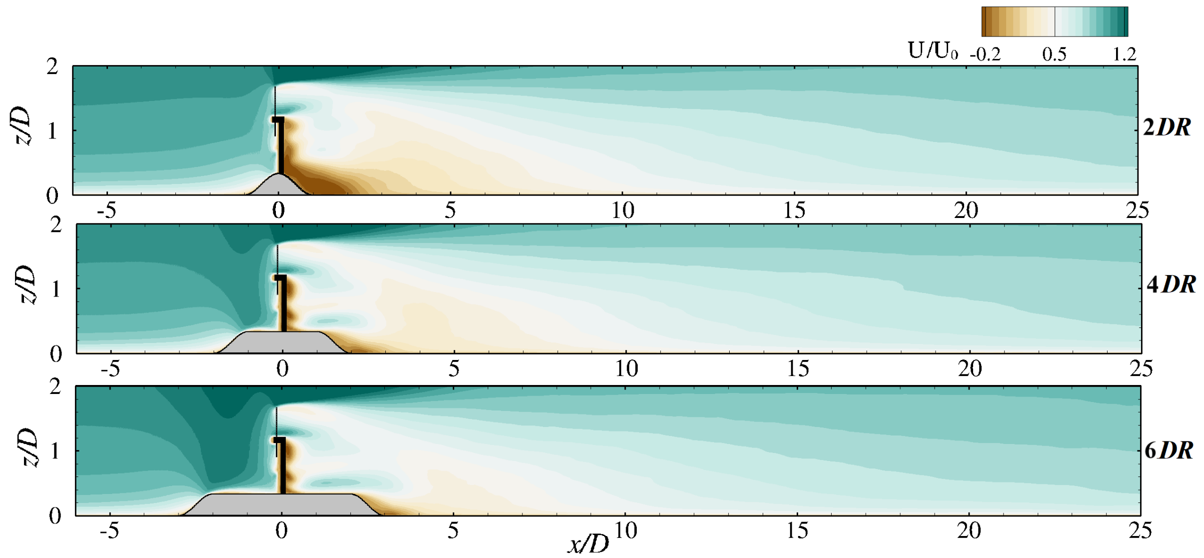

Fig. 5. Normalised mean streamwise velocity contours over $xz-$plane for the turbines located on ridge tops (TC).

and to less than 2% difference in velocity fluctuations. However, the wake of these turbines would experience a flow acceleration approaching the ridge top that will contribute to a faster wake recovery together with the high shear developed downstream of the ridge, observed in the increased levels of turbulence intensity and Reynolds shear stress in Fig. 2.

For turbines located at the centre of the ridge top (TC) at $x/D = 0$, the vertical distribution of the streamwise velocity is approximately uniform across the water depth. At this location, the disc-averaged velocity is increased by 19%, 23% and 24% from the undisturbed depth averaged velocity at the $2DR$, $4DR$ and $6DR$ cases, respectively, as seen in Table I. At the same location, Fig. 3b shows an increase in turbulence intensity near the bottom for $4DR$ and $6DR$ cases over the ridge's flat surface. This increase is due to the high shear induced by the wake downstream of the crest of the ridge's leading edge which decreases with distance downstream [27].

Turbines downstream of the ridge (TD) are expected to be subjected to a highly-sheared mean velocity profile that has lower values below the bottom tip of the turbine compared to the other locations. This flow shear is steeper for the $2DR$ case. Furthermore, Table I shows that the disc-averaged velocity and turbulence intensity for TD turbines decrease as ridge length increases. This is due to the recirculation region in the lee side of the ridge, which causes high velocity fluctuations and intense turbulent momentum

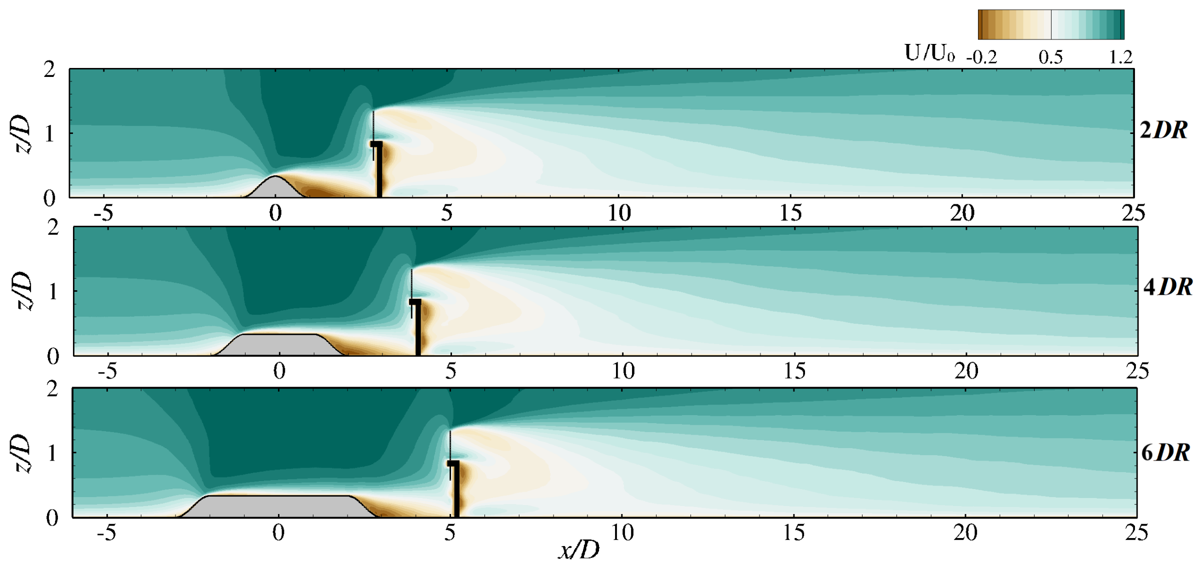

Fig. 6. Normalised mean streamwise velocity contours over $xz-$plane for the downstream turbines (TD).

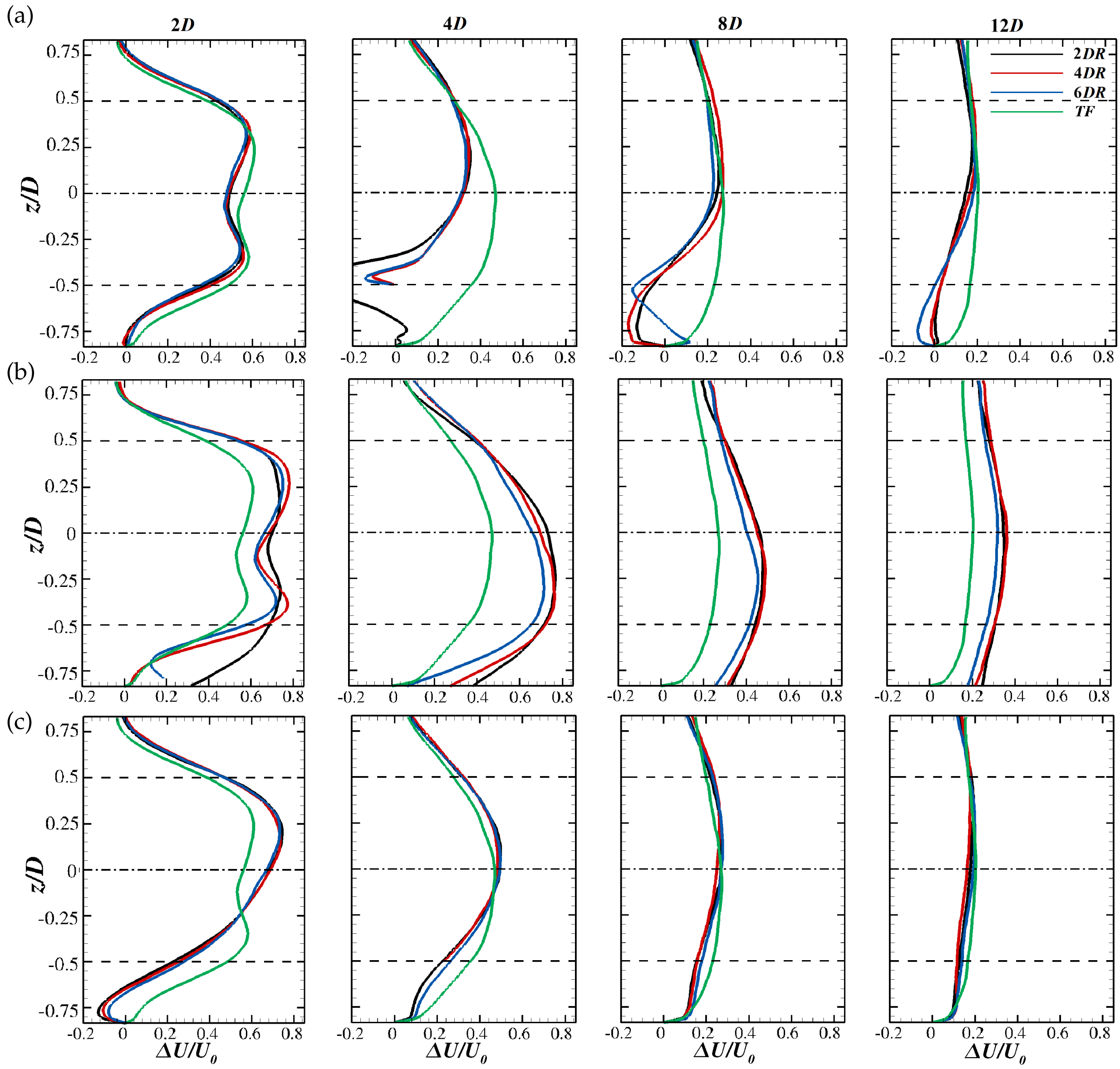

Fig. 7. Vertical distribution of velocity deficit at $2D, 4D, 8D$ and $12D$ downstream of the rotor for (a) upstream turbines and the flat-bed case, (b) turbines at ridge centre and (c) downstream turbines. Black dashed line shows the turbine area and turbine centre is used as a local coordinate reference in the $z-$axis.

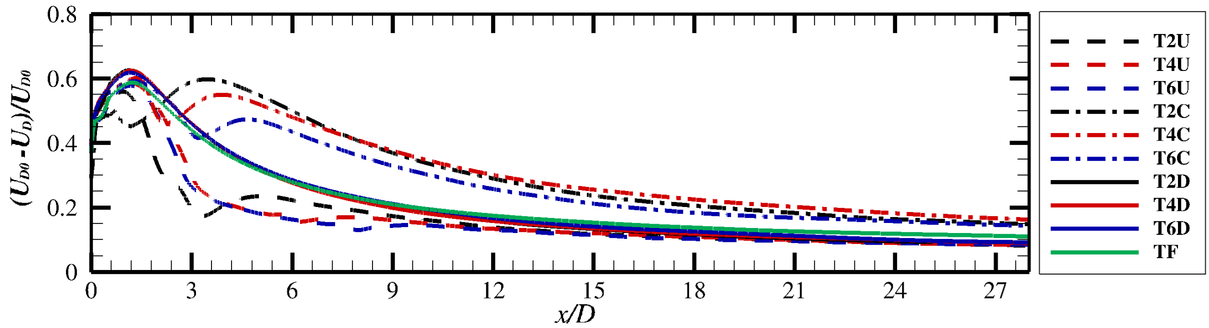

Fig. 8. Disc-averaged velocity deficit normalised by the disc-averaged velocity of the flow with no-turbine.Turbines are located at $x/D = 0$.

exchange due to the shear layer formed there. The effect of the recirculation region is more pronounced in the $2DR$ ridge case as the flow is deflected upwards over the lee side of the ridge. Whereas for the elongated ridges ($4DR$ and $6DR$), the flow deflected from the upstream ridge slope is recovered over the flat surface on the ridge top and therefore the recirculating flow downstream of the ridge is reduced.

B. Wake deficit

The distribution of mean velocity in the presence of the turbine is shown in Fig. 4 for the flat-bed case and upstream turbines. For all of the considered ridge lengths, it can be seen that the slow wake flow generated by the turbine is reduced at the ridge leading edge due to the effect of the favorable pressure gradient. However, downstream of the ridge, turbine wakes merge with the ridge wake which contributes to the overall flow reduction in this region.

To analyse this further, vertical profiles of velocity deficit ($\triangle U$) at $2D, 4D, 8D$ and $12D$ downstream of the rotor are presented in Fig. 7. The deficit is calculated by removing the flow field from the simulation with no turbine from that in which a turbine is simulated, in order to isolate the ridge wake from turbine wake. Thus the velocity deficit is computed as $\triangle U(x, y, z) = U_{NT}(x, y, z) - U_T(x, y, z)$, where U_{NT} and U_T denote the mean streamwise velocity in the absence and presence of a turbine, respectively. Fig. 7a shows the vertical distribution of velocity deficit for the flat-bed and TU cases. It can be seen that at $4D$, the deficit is reduced by approximately 75% from the depth-averaged velocity, whereas this reduction is achieved at approximately $8D$ for the flat-bed case. A negative deficit is observed in the lower half of the wake for the ridge cases, which indicates that the flow in the presence of the turbine is faster than the flow over the ridge alone. This is due to the bypass flow around the turbine, which is deflected upwards over the ridge region.

Fig. 5 shows the mean velocity distribution for turbines sited at the ridge top. At this location, turbine wakes are likely to extend for a long distance downstream of the turbine due to the adverse pressure gradient generated in the lee side of the ridge. Vertical profiles for TC turbines (see Fig. 7b) show that the wake persists for a longer distance compared to turbine wakes in the other locations or in the flat-bed case. At a distance of $12D$, approximately 35% of velocity deficit is reached for TC cases compared to 20% for TD turbines, as seen in Fig. 7. It is noteworthy that in the case of $6DR$, the observed wake deficit is slightly lower than in the case of $4DR$ and $2DR$. This could be attributed to the longer distance between the turbine and the adverse pressure side of the ridge.

For the downstream turbines shown in Fig. 6, velocity distribution downstream of the turbine show similar distribution for all ridge lengths, again seen in Fig. 7c with almost identical profiles of velocity deficit. However, comparing to the flat-bed case, wake recovery for TD turbines is similar to the flat-bed case beyond $8D$ although this location is subjected to higher turbulence intensity comparing to the flat-bed and a faster wake recovery is expected. This observation could be attributed to the accelerated flow induced by the ridge presence (see Fig. 6), therefore, the wake of turbines in this location is under adverse pressure gradient.

To analyse wake recovery with downstream distance, Fig. 8 shows the disc-averaged velocity deficit evolution along the downstream direction normalised by the disc-averaged velocity with no turbine. For the flat-bed case, the velocity deficit remains approximately 15% at $15.4D$ downstream of the turbine, i.e. 85% wake recovery. A similar velocity deficit is found at downstream distances of $10.9D$, $10D$, and $6.8D$ for TU locations in the $2DR$, $4DR$, and $6DR$ cases respectively, whereas for TC locations, a 15% velocity deficit threshold is achieved further downstream at a distances beyond $25D$ compared to the flat-bed case. Considering turbines downstream of the ridge, similar to the observations in Fig. 7, TD locations show a similar trend in wake recovery to the flat-bed case; however, 15% of velocity deficit is attained closer to the turbine by $1.7D$ in the case of $6DR$, and by $2.6D$ in the case of $4DR$ and $2DR$ when compared to the flat-bed case.

C. Fatigue loads

Fatigue loads acting on the turbine structure are determined using Damage Equivalent Loads (DELs) [28]. A rainflow cycle counting method [29] is used to identify the range of load cycles experienced by the turbine blades over the operation time. The time history of the forces computed with the ALM are analysed and the DELs are calculated using the number

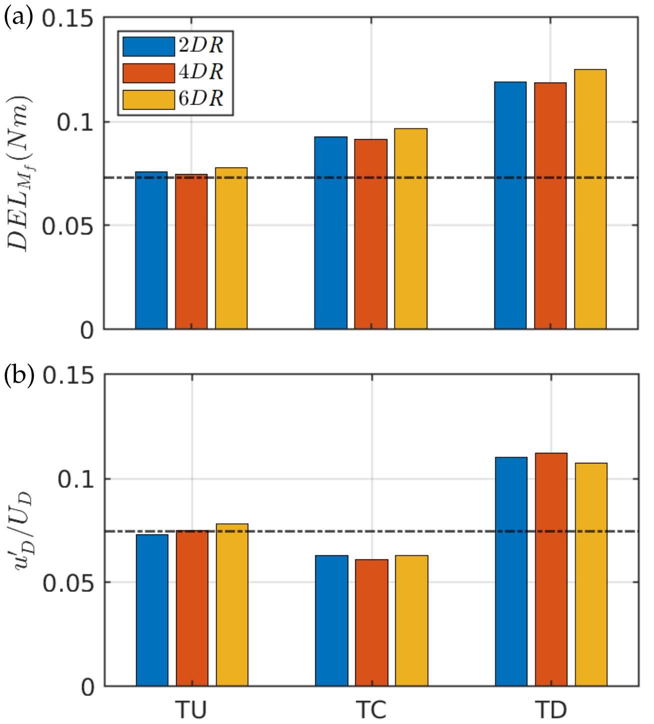

Fig. 9. Comparison of three ridges of (a) Damage Equivalent Loads (DELs) of flapwise bending moment acting on a single blade and (b) disc-averaged turbulence intensity normalised by the disc-averaged mean velocity for the tested case. The black dashed-dotted line shows the values for the flat-bed case.

of load cycles and the load range over the simulated turbine revolutions following the formula:

$$DEL = \left(\frac{\sum_i n_i F_i^m}{N} \right)^{\frac{1}{m}} \tag{3}$$

where for every bin i, the variables n_i and F_i represent the number of load cycles and load range, respectively, m is the material property, and N is the number of turbine rotations.

Fig. 9 illustrates the DELs of the flapwise bending moment M_f acting on a single blade and the disc-averaged turbulence intensity normalised by the disc-averaged mean velocity. The DELs for the upstream turbines are similar to that for the flat-bed case (shown in black dashed-dotted line), as the flow conditions in these areas are comparable. However, the DELs for turbines located on ridge tops (locations TC) show a slight increase, which can be attributed to the high mean load value resulting from the accelerated flow. Despite this increase, the velocity fluctuations at these locations are approximately similar to those for upstream turbines (see Table I). In contrast, downstream turbines exhibit the highest DELs, due to both the high load values and fluctuations present in these areas.

V. Conclusion

In this study, the influence of symmetric ridges on the wake and loading of a single tidal stream turbine is assessed through large-eddy simulations of a laboratory-scale turbine located at different positions relative to three different ridge lengths. The results show that the turbine wake recovers more rapidly when the turbine is located a short distance upstream of a symmetric ridge, with the distance to a deficit recovery of 15% reduced to $10.9D$ in the short ridge length, approximately 29% shorter than for the wake of the same turbine over a flat-bed. This distance reduces further for increased ridge length, up to about 55% smaller than the flat-bed for the longest ridge length studied. For turbines located at ridge top, much longer wakes are observed compared to other locations, with a slight decrease of recovery distance for longer ridges. The wake from turbines located downstream of the ridge recovers at a very similar rate to that observed from turbines operating over a flat surface.

Analysis of fatigue loads acting on rotor blades indicate that turbines located on the top of a ridge experience high mean load due to deployment in a region of accelerated flow, whilst turbines downstream of a ridge are subjected to greater fatigue loads due to operation in region with elevated levels of turbulence. Considering a full tidal cycle with the assumption that the flow statistics are similar in both directions, locations TU and TD would represent the same turbine in opposing cycles and the aggregated damage equivalent loads could be higher at locations to the side of the ridge than at the ridge top. These results outline the need for detailed analyses of relative turbine locations in proximity to bathymetric features such as ridges.

These findings suggest that for a multi-row tidal stream array, a ridge between rows could have a positive impact in terms of wake recovery rate such that the downstream turbines would be less affected by the upstream turbine wake. Conversely, fatigue loads for turbines downstream of a ridge are increased due to ridge induced turbulence. Further analysis is required for tidal turbine arrays to quantify fatigue loads on secondary row turbines in both the presence and absence of a ridge.

Acknowledgement

Authors would like to acknowledge the assistance given by Research IT and use of Computational Shared Facility (CSF) at The University of Manchester. The authors gratefully acknowledge the help of the ARCHER2 UK National Supercomputing Service (https://www.archer2.ac.uk).

References

[1] P. Mercier, M. Grondeau, S. Guillou, J. Thiébot, and E. Poizot, "Numerical study of the turbulent eddies generated by the seabed roughness. case study at a tidal power site," *Applied Ocean Research*, vol. 97, p. 102082, 2020.

[2] M. Harrold and P. Ouro, "Rotor loading characteristics of a full-scale tidal turbine," *Energies*, vol. 12, no. 6, p. 1035, 2019.

[3] M. Togneri and I. Masters, "Micrositing variability and mean flow scaling for marine turbulence in Ramsey Sound," *Journal of Ocean Engineering and Marine Energy*, vol. 2, pp. 35–46, 2016.

[4] A. C. Bourgoin, S. S. Guillou, J. Thiébot, and R. Ata, "Turbulence characterization at a tidal energy site using large-eddy simulations: case of the Alderney Race," *Philosophical Transactions of the Royal Society A*, vol. 378, no. 2178, p. 20190499, 2020.

[5] S. Shamsoddin and F. Porté-Agel, "Wind turbine wakes over hills," *Journal of Fluid Mechanics*, vol. 855, pp. 671–702, 2018.

[6] L. Liu and R. J. Stevens, "Effects of two-dimensional steep hills on the performance of wind turbines and wind farms," *Boundary-Layer Meteorology*, vol. 176, no. 2, pp. 251–269, 2020.

[7] W. Tian, K. Zheng, and H. Hu, "Investigation of the wake propagation behind wind turbines over hilly terrain with different slope gradients," *Journal of Wind Engineering and Industrial Aerodynamics*, vol. 215, p. 104683, 2021.
[8] Z. Zhang, P. Huang, G. Bitsuamlak, and S. Cao, "Large-eddy simulation of wind-turbine wakes over two-dimensional hills," *Physics of Fluids*, vol. 34, no. 6, p. 065123, 2022.
[9] H. Mullings and T. Stallard, "Assessment of dependency of unsteady onset flow and resultant tidal turbine fatigue loads on measurement position at a tidal site," *Energies*, vol. 14, no. 17, p. 5470, 2021.
[10] P. Ouro and T. Stoesser, "Impact of environmental turbulence on the performance and loadings of a tidal stream turbine," *Flow, Turbulence and Combustion*, vol. 102, no. 3, pp. 613–639, 2019.
[11] B. Gaurier, M. Ikhennicheu, G. Germain, and P. Druault, "Experimental study of bathymetry generated turbulence on tidal turbine behaviour," *Renewable Energy*, vol. 156, pp. 1158–1170, 2020.
[12] P. Mercier and S. S. Guillou, "Spatial and temporal variations of the flow characteristics at a tidal stream power site: A high-resolution numerical study," *Energy Conversion and Management*, vol. 269, p. 116123, 2022.
[13] P. K. Stansby and P. Ouro, "Modelling marine turbine arrays in tidal flows," *Journal of Hydraulic Research*, vol. 60, no. 2, pp. 187–204, 2022.
[14] P. Mycek, B. Gaurier, G. Germain, G. Pinon, and E. Rivoalen, "Experimental study of the turbulence intensity effects on marine current turbines behaviour. Part II: Two interacting turbines," *Renewable Energy*, vol. 68, pp. 876–892, 2014.
[15] X. Yang, K. B. Howard, M. Guala, and F. Sotiropoulos, "Effects of a three-dimensional hill on the wake characteristics of a model wind turbine," *Physics of Fluids*, vol. 27, no. 2, p. 025103, 2015.
[16] T. Blackmore, L. E. Myers, and A. S. Bahaj, "Effects of turbulence on tidal turbines: Implications to performance, blade loads, and condition monitoring," *International Journal of Marine Energy*, vol. 14, pp. 1–26, 2016.
[17] K. Røkenes and P.-Å. Krogstad, "Wind tunnel simulation of terrain effects on wind farm siting," *Wind Energy*, vol. 12, no. 4, pp. 391–410, 2009.
[18] P. Ouro, L. Ramírez, and M. Harrold, "Analysis of array spacing on tidal stream turbine farm performance using large-eddy simulation," *Journal of Fluids and Structures*, vol. 91, p. 102732, 2019.
[19] P. Ouro, M. Harrold, L. Ramirez, and T. Stoesser, "Prediction of the wake behind a horizontal axis tidal turbine using a LES-ALM," in *Recent Advances in CFD for Wind and Tidal Offshore Turbines*. Springer, 2019, pp. 25–35.
[20] F. Nicoud and F. Ducros, "Subgrid-scale stress modelling based on the square of the velocity gradient tensor," *Flow, turbulence and Combustion*, vol. 62, no. 3, pp. 183–200, 1999.
[21] M. Uhlmann, "An immersed boundary method with direct forcing for the simulation of particulate flows," *Journal of computational physics*, vol. 209, no. 2, pp. 448–476, 2005.
[22] A. M. Roma, C. S. Peskin, and M. J. Berger, "An adaptive version of the immersed boundary method," *Journal of computational physics*, vol. 153, no. 2, pp. 509–534, 1999.
[23] W. Z. Shen, J. N. Sørensen, and R. Mikkelsen, "Tip loss correction for actuator/navier–stokes computations," *J. Sol. Energy Eng.*, vol. 127, no. 2, pp. 209–213, 2005.
[24] M. J. Churchfield, S. J. Schreck, L. A. Martinez, C. Meneveau, and P. R. Spalart, "An advanced actuator line method for wind energy applications and beyond," in *35th Wind Energy Symposium*, 2017, p. 1998.
[25] T. Stallard, T. Feng, and P. Stansby, "Experimental study of the mean wake of a tidal stream rotor in a shallow turbulent flow," *Journal of Fluids and Structures*, vol. 54, pp. 235–246, 2015.
[26] L. Chen, K. Asai, T. Nonomura, G. Xi, and T. Liu, "A review of backward-facing step (bfs) flow mechanisms, heat transfer and control," *Thermal Science and Engineering Progress*, vol. 6, pp. 194–216, 2018.
[27] A. Bowen and D. Lindley, "A wind-tunnel investigation of the wind speed and turbulence characteristics close to the ground over various escarpment shapes," *Boundary-Layer Meteorology*, vol. 12, no. 3, pp. 259–271, 1977.
[28] G. McCann, "Tidal current turbine fatigue loading sensitivity to waves and turbulence–a parametric study," in *Proceedings of the 7th European Wave and Tidal Energy Conference*, 2007.
[29] ASTM International, "Standard practices for cycle counting in fatigue analysis," West Conshohocken, PA, 2017, aSTM E1049-85(2017). [Online]. Available: https://www.astm.org/e1049-85r17.html